Nonlinear Finite Element Analysis of Polypropylene Lightweight RC Beams

Shimaa M. Mahmoud [a], Mohamed E. El-Zoughiby [a], Ahmed A. Mahmoud [b], Mohammed A. Abd Elrahman[a]

[a] **Structural Engineering Department, Faculty of Engineering, Mansoura University, Egypt**

[b] **Professor, Faculty of Engineering (Shoubra), Benha University, Egypt (E-mail: ahmed.m5882@gmail.com)**

ABSTRAT

The main objective of this research is to investigate nonlinearly the flexural behavior of Polypropylene Fiber (PF) Lightweight RC beams. The finite element (FE) method utilizing ANSYS program was used to build the models and study the effects of some parameters on the response of PF lightweight RC beams in flexure. The considered parameters include the effect of main steel and its yield strength, beam width, beam depth and shear span. The obtained results were compared with those calculated based on the ACI 318-19 and the AS 3600-2018 design building codes and the comparison showed a great match between results, especially the ACI 318-19 code.

Keywords: polypropylene fiber, lightweight concrete, nonlinear finite element, flexural behavior.

1. INTRODUCTION

Lightweight concrete has a lower density than normal concrete, which ranging from 320 to 1920 kg/m3 [1]. It reduces structural mass, lowering foundation costs and improving thermal and sound insulation properties. Despite its many advantages, lightweight concrete has a low tensile strength, therefore, fibers are used to compensate for this [2]. Polypropylene fibers (PF) can increase structural strength, ductility and reduce crack widths and tightly controlling crack widths [2-5]. Srinivasu et al. [5] studied the effect of PF on the behavior lightweight concrete and the addition of PF showed better effect on the concrete tensile strength. Gencel et al. [6] investigated the mechanical properties of self-compacting PF lightweight reinforced concrete. The use of PF decreased unit weight while improving the hardened properties of PF reinforced lightweight concrete. Also, Mazaheripour et al. [7] investigated the influence of PF on lightweight concrete. The results revealed that the tensile and flexural strength increased by approximately 14.4% and 10.7%, respectively.

Additionally, Altalabani et al. [8] investigated the mechanical properties of self-compacting lightweight concrete with PF that slightly improved the elastic modulus and the splitting tensile strength.

Because experimental tests take a long time and are expensive, it was essential for the researchers to find less expensive methods, so they turned to use various methods of modeling concrete structures using both numerical and analytical methods [9, 10]. Finite element (FE) analysis is used for structure assessment and provides precise and quick results when compared to experimental studies. Many researchers have used FE method to study the behavior of concrete elements [11-13]. Musmar [11] investigated the flexural behavior of RC beams and compared the results to that obtained using ACI 213-14 [1] code. The results demonstrated that FE modeling provided more objective simulation of the experimental procedure. The flexural behavior of RC beams was numerically investigated by Tjitradi et al. [12]. Accordingly, they concluded that FE is a good tool for analyzing beams and producing accurate results when compared to experimental results. Amna et al. [13] used FE method to simulate lightweight RC beams. The numerical results yield appropriate solution. Many researchers have compared the experimental results of normal concrete with the FE results. The aim of this research is to numerically study the flexural behavior of polypropylene lightweight concrete reinforced beams using ANSYS program. For verification purposes, the obtained results are, then, compared with those obtained based on the two building codes of ACI 318-19 [14] and AS 3600-2018 [15].

2. NONLINEAR FINITE ELEMENT ANALYSIS

As shown in Fig. 1, PF lightweight concrete was modeled by the element SOLID65 with eight nodes, each has three degrees of freedom. Table 1 shows the stress-strain for Polypropylene Light-Weight Concrete (PLWC) in compression using standard cylinder according to (ASTM C 39) which experimentally evaluated by the first author [17]. The element LINK180 was used to model steel reinforcement. It has 2-nodes. The element SOLID185 was used to model the steel plates and has eight nodes. The material properties of the considered and previously tested beams are shown in Table 2. Figure 2 shows the FE modeling of the considered beams. The model consists of horizontal and vertical strips according to the number of bottom and top reinforcement, spacing of stirrups, and concrete cover. The bond between steel and concrete is assumed to be perfected bond. Due to symmetry, half of the beam was modeled considering the boundary conditions shown in Fig. 3. Four steel plates were modeled using element SOLID 185. The applied loads were distributed across the centerline of the two plates at the top of the beam.

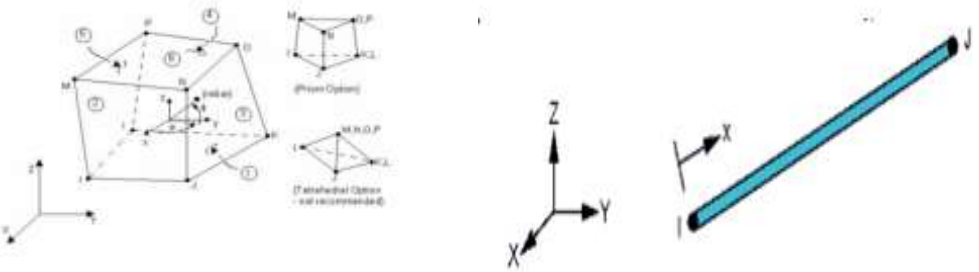

(a) SOLID65. (b) LINK180.

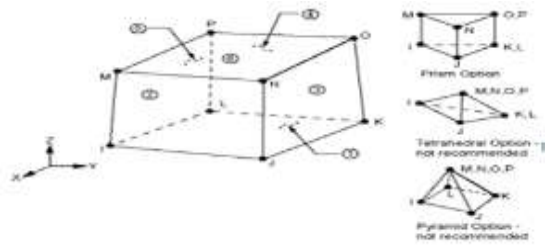

(c) SOLID185.

Fig. 1 Element Geometry [16].

Table 1 The stress-strain for Polypropylene Light-Weight Concrete (PLWC) in compression using standard cylinder according to ASTM C 39 [17].

Point	Strain (%)	Stress (MPa)
1	0.02	2.83
2	0.06	8.49
3	0.0806	11.3
4	0.1046	14.15
5	0.1333	16.98
6	0.197	22.64
7	0.28	26

Table 2 Material properties of the studied and previously tested beams.

Material	E (GPa)	ν (-)	$f_c^{`}$ (MPa)	f_t (MPa)	f_y (MPa)	E_t (GPa)	Open shear transfer coef.	Closed shear transfer coef.
Concrete	14	0.2	26	2.8	---	---	0.2	1.0
Steel reinforcement for the considered beams	200	0.3	---	---	360	20	---	---
Steel reinforcement for tested beams	200	0.3	----	---	400	20	---	---
Supports and loading plates	2000	0.25	----	---	----	-----	------	-----
Where : E = Modulus of elasticity, ν = Poisson's ratio, $f_c^{`}$ = Concrete strength, f_t = Tensile splitting strength, f_y = Yield strength and E_t = Tangent modulus								

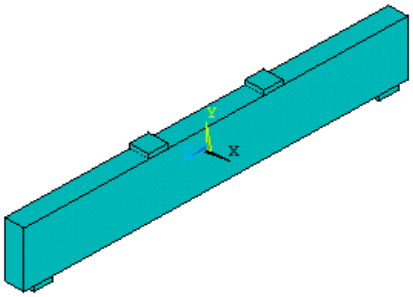

(a) The creation of the model.

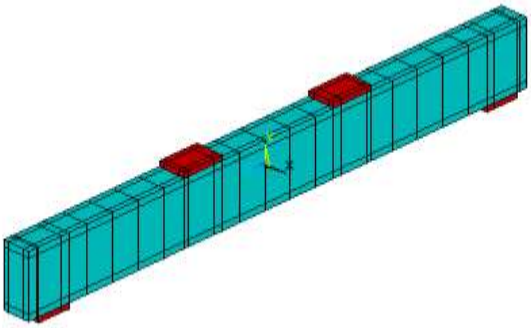

(b) Vertical and horizontal strips.

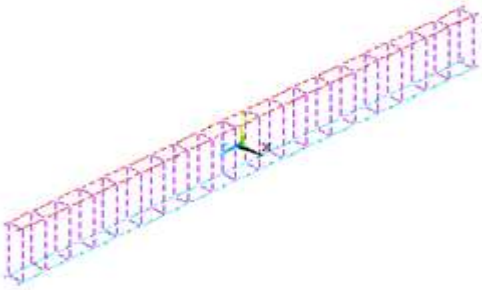

(c) Meshing of steel reinforcement.

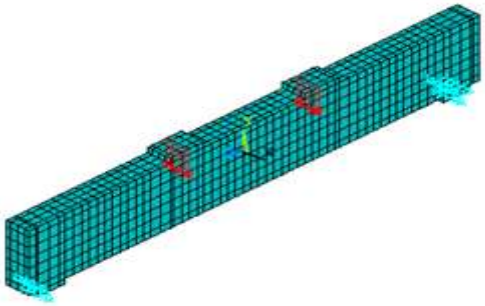

(d) Meshing of beam and boundary conditions.

Fig. 2 Finite element modeling of considered beams.

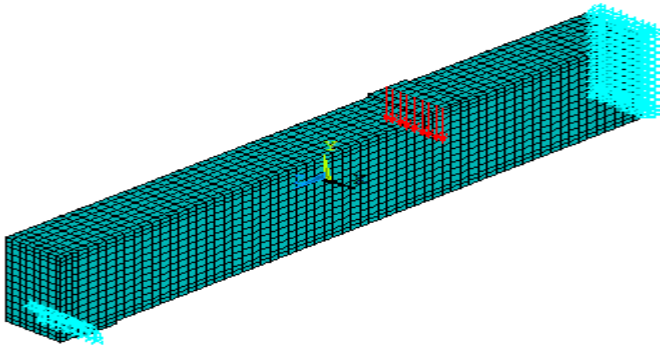

Fig. 3 Half of the model with boundary conditions.

3. VERIFICATION

3.1 Details of studied beams

The beams previously tested by the author [17] were used to verify the numerical output results. Many mixes have been designed on polypropylene fiber lightweight concrete to obtain the desired strength. Pure PF was used in the experiment and had a density of 910 kg/m^3, a tensile strength of 370 MPa, an elasticity modulus of 3750 MPa and an aspect ratio of 90. The volume content of PF was 0.1% of concrete volume. The strength of the used mix is 31MPa for cube and 26MPa for cylinder after 28 days. The modulus of elasticity of the used concrete was 14 GPa. Figure 4 shows the dimensions and

reinforcement details of beam B1. The beam cross section is 100 mm width and 300 mm depth and its clear span is 1800 mm. The beams have been tested until failure and the shear span-to-total beam depth ratio (a/t) was 2.0.

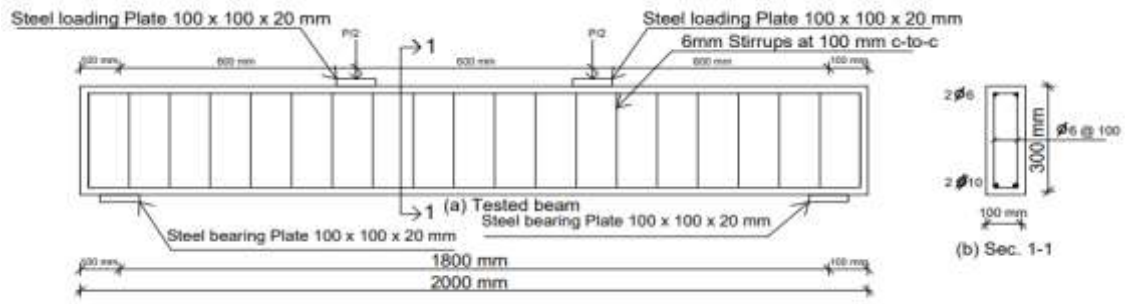

Fig. 4 Typical dimensions and reinforcement details of beam B1 [17].

3.2 The experimental and numerical results

Upon comparing the experimental and numerical results for the beam B1 as shown in Figure 5 for the load-deflection curve and as in Table 3 for ultimate load, deflection at ultimate load, and secant stiffness, the following conclusions can be drawn:

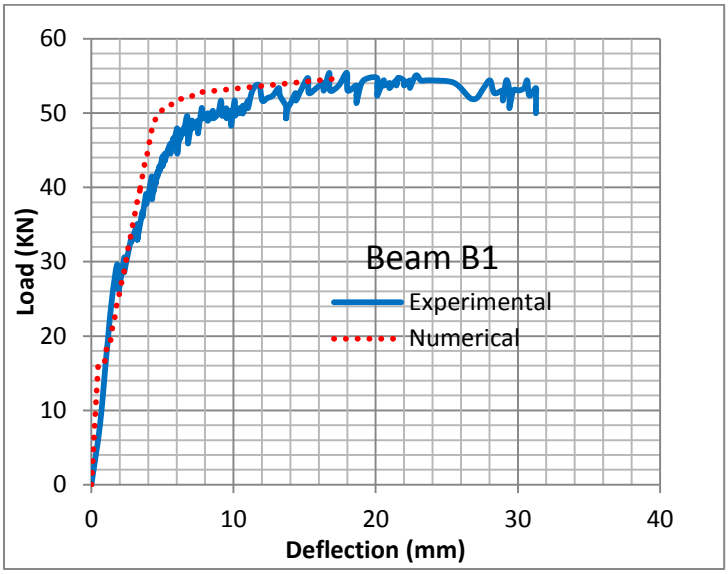

Fig. 5 Experimental vs. numerical load-deflection curve for beam B1.

Table 3 Comparison between the numerical and the experimental results of beam B1.

Comparison	Exp. [17]	FE	Exp. / FE
Ultimate load P_u, kN	55.42	54.6	1.01
Deflection at ultimate load Δ_u, mm	17.97	17.0	1.05

Secant stiffness, kN/mm	3.08	3.2	0.96

1. The FE predictions have been close to the experimental results at the ultimate level.

2. For the considered beam B1, the ratio (P_u^{EXP}/P_u^{FE}) is 1.01, the ratio ($\Delta_u^{EXP}/\Delta_u^{FE}$) is 1.05, and the ratio of the experimental to FE secant stiffness cracking load is 0.96.

AS Fig. 6 illustrates, the early flexural cracks appeared at the middle of the beam span and propagated as the load increased. Figure 6 shows, also, a very good agreement between the experimental and the numerical crack patterns.

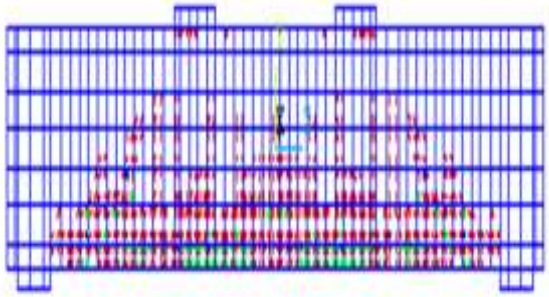

(a) Predicted crack pattern.

(b) Experimental crack pattern.

Fig. 6 Experimental and predicted crack pattern for beam B1.

4. PARAMETRIC NUMERICAL STUDY

4.1 Details of studied beams

Figure 7 shows the geometry and reinforcement details of the parametric studied beams. Five groups are considered as in Table 4 and nonlinearly analyzed using ANSYS program. The used two hangers were 2Φ12 whereas the stirrups were 10Ø8/m. The first group represented the effect of main steel reinforcement; that is 3Φ22, 3Φ25 and 4Φ25 for beams B2, B3 and B4, respectively. The beam B2 was considered a control (or reference) beam. The second group represented the effect of reinforcement steel yield strength f_y, which was 400, 500 and 600 MPa for beams B5, B6 and B7, respectively. The third group represented the effect of beam width *b*; 240 and 360 mm for beams B8 and B9, respectively. The fourth group represented the effect of beam depth *t*; 720 mm and 840 mm for beams B10 and B11, respectively. The last group represented the effect of shear span *a*; 1500 and 2500 mm with shear span-to-span ratio equals 0.25 and 0.417 for beams B12 and B13, respectively.

Table 4 Details of the studied beams.

Group	Beam No.	Main steel	f_y, (MPa)	b (mm)	t (mm)	a (mm)	Notes
1	**B2**	3Φ22	360	300	600	2000	Effect of main steel ratio (μ)
	B3	3Φ25	360	300	600	2000	
	B4	4Φ25	360	300	600	2000	
2	**B5**	3Φ22	400	300	600	2000	Effect of (f_y)
	B6	3Φ22	500	300	600	2000	
	B7	3Φ22	600	300	600	2000	
3	**B8**	3Φ22	360	240	600	2000	Effect of beam width (b)
	B9	3Φ22	360	360	600	2000	
4	**B10**	3Φ22	360	300	720	2000	Effect of beam depth (t)
	B11	3Φ22	360	300	840	2000	
5	**B12**	3Φ22	360	300	600	1500	Effect of shear span (a)
	B13	3Φ22	360	300	600	2500	

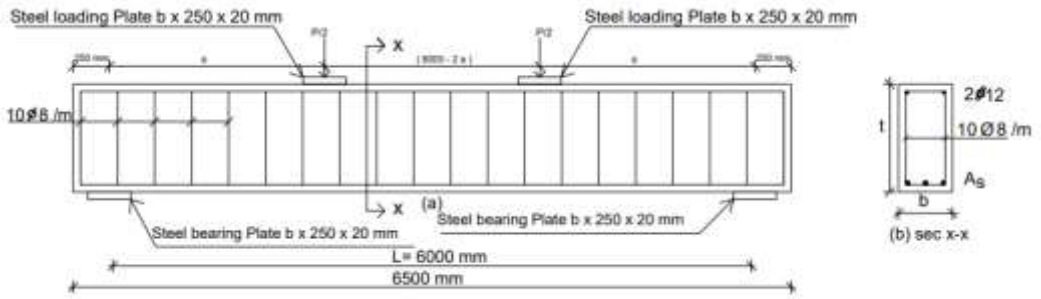

Fig. 7 Geometry and reinforcement details of the parametric studied beams.

4.2 Numerical results

The load-deflection curve depicts the behavior of the beams by displaying a variety of response parameters, including ultimate load, deflection, and secant stiffness. Figure 8 and Table 5 show the effect of these parameters on the behavior of PF lightweight concrete.

Table 5 Numerical results of the studied beams.

Beam No.	Numerical ultimate load P_u (kN)	Deflection at ultimate load Δ_u (mm)	Secant stiffness (kN/mm)	$\frac{P_u}{P_u^{B2}}$ (%)	$\frac{\Delta_u}{\Delta_u^{B2}}$ (%)	Secant stiffness relative to that of B2 (%)
B2	227.80	42.8	5.32	100.00	100.00	100.00
B3	276.10	37.4	7.38	121.20	87.38	138.72
B4	328.90	29.6	11.10	144.38	69.16	208.65
B5	242.50	42.2	5.75	106.45	98.60	108.08
B6	292.70	38.5	7.60	128.49	89.95	142.86
B7	332.50	38.3	8.68	145.96	89.49	163.16
B8	200.10	37.9	5.27	87.84	88.55	99.06
B9	242.50	43.0	5.64	106.45	100.47	106.02
B10	251.70	27.9	9.02	110.49	65.19	169.55
B11	335.00	22.3	15.02	147.06	52.10	282.33
B12	316.00	43.7	7.23	138.72	102.10	135.90
B13	170.00	27.3	6.23	74.63	63.79	117.11

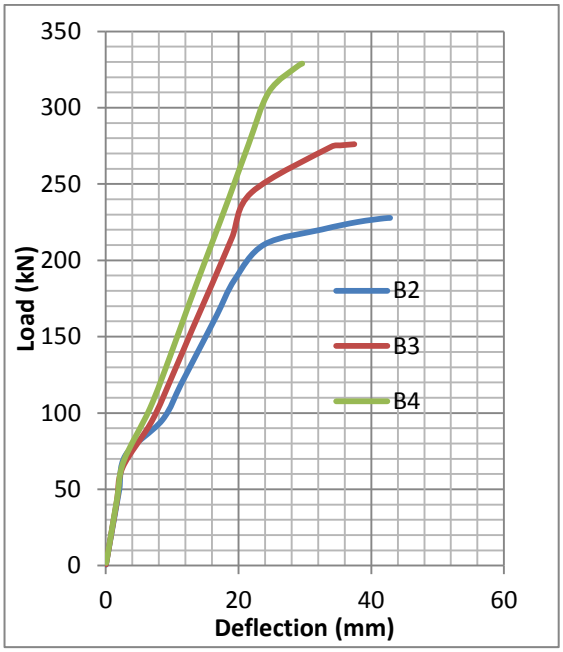

(a) Effect of main steel.

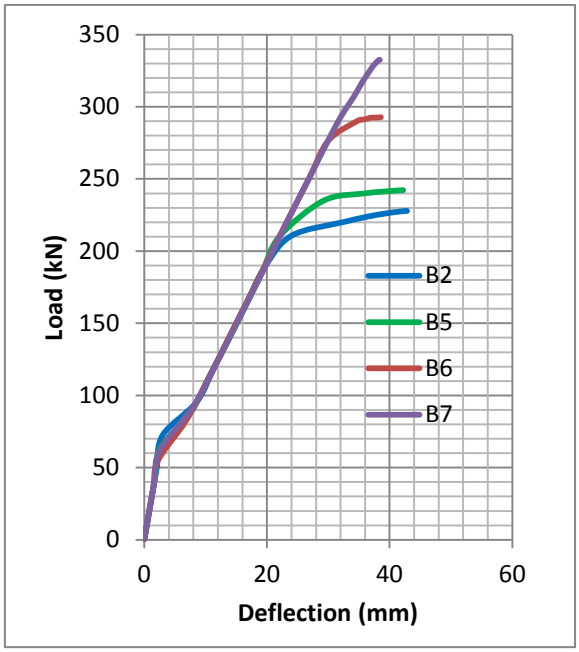

(b) Effect of steel yield strength.

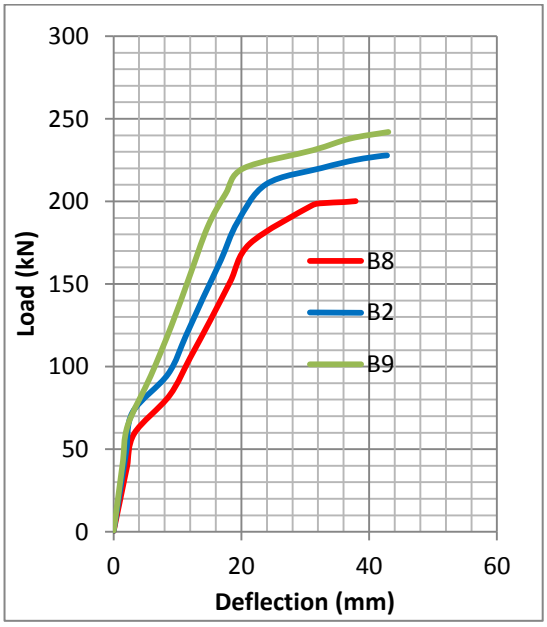

(c) Effect of beam width.

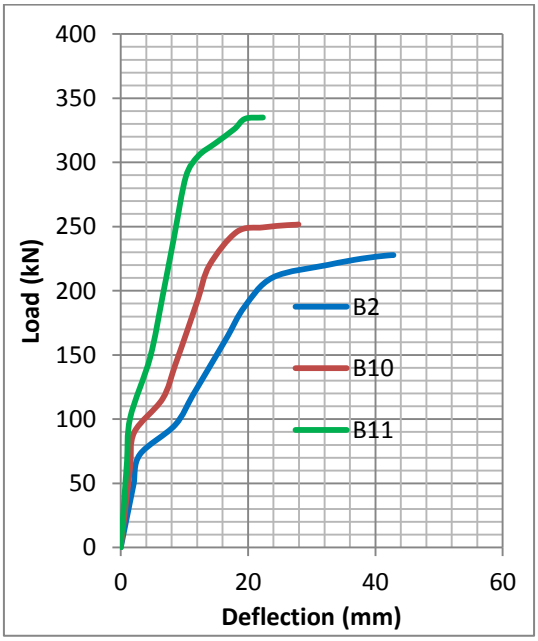

(d) Effect of beam depth.

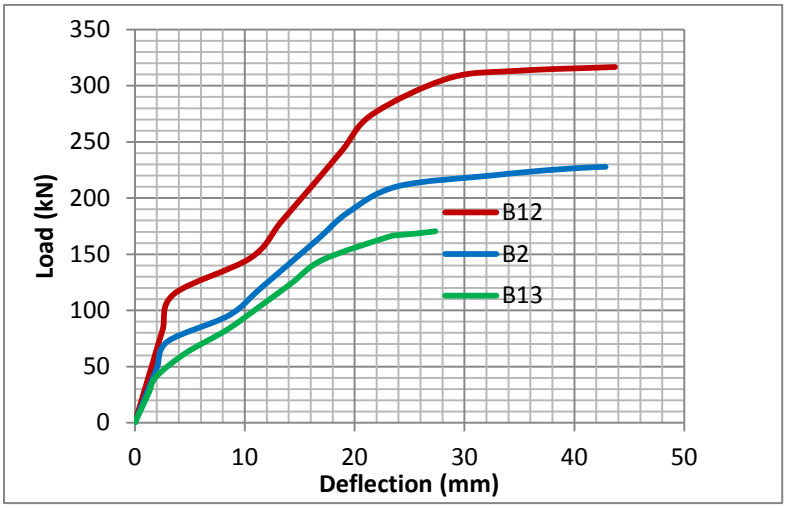

(e) Effect of shear span.

Fig. 8 Load-deflection curve of all parametric studied beams.

4.3 Effect of main steel

Table 5 shows the effect of changing the main steel on the behavior of PF lightweight concrete for the three beams B2, B3 and B4. The ultimate load of beams B3 and B4 is greater than that of beam B2 by 21.2% and 44.38%, respectively. The secant stiffness of beams B3 and B4 is greater than that of beam B2 by 38.72% and 108.65%, respectively. The deflection of beams B3 and B4 is smaller than the deflection of beam B2 by 12.62% and 30.84%, respectively. As a result as shown in Fig. 8, the higher the main steel, the higher the ultimate load, the higher secant stiffness and the lower the corresponding deflection.

4.4 Effect of steel yield strength

Four beams were modeled and analyzed using ANSYS program to study the effect of steel yield strength, f_y. The yield strength f_y was taken 360, 400, 500 and 600 MPa for beams B2, B5, B6 and B7, respectively. As Fig. 8 illustrates the initial parts of the load deflection curves are approximately similar to those of group 2. But they are varied nearest to the ultimate load according to the value of the steel yield strengthf_y. Based on Table 5, the ultimate load of beams B5, B6 and B7 is larger than that of beam B2 by 6.45%, 28.49% and 45.96%, respectively. The secant stiffness of beams B5, B6 and B7 is larger than that of beam B2 by 8.08%, 42.86% and 63.16%, respectively. The corresponding deflections are smaller than that of beam B2 by 1.40%, 10.05%, and 10.51%, respectively. Clearly, the higher the yield strengthf_y, the higher the ultimate load, the higher secant stiffness and the lower the deflection.

4.5 Effect of beam width and depth

Figure 8 shows the load deflection curves of beams B2, B8, B9, B10 and B11 for studying the effect of changing beam width and depth. Obviously, increasing the beam depth and width increases the ultimate load, increases the secant stiffness and decreases the deflection. The secant stiffness of beams B9, B10 and B11 is greater than that of B2 by 6.02%, 69.5% and 182.32%, respectively.

4.6 Effect of shear span

To account for its effect, the shear span *a* is taken 1500, 2000, and 2500 mm for beams B12, B2, and B13, respectively, as shown in Table 5 . The load deflection curves in Figure 8 illustrate the effect of shear span *a* on the behavior of PF lightweight concrete. The ultimate load of beam B12 is greater than that of beam B2 and the ultimate load of beam B13 is smaller than that of beam B2 by 38.72% and 25.37%, respectively. The deflection of beam B12 is greater than that of B2 and the deflection of B13 is smaller than that of B2 by 2.10% and 36.21%, respectively. Obviously, the higher the beam shear span, the lower the ultimate load and deflection and the higher secant stiffness.

5. Numerical results compared to those calculated based on ACI318-19 and AS 3600-2018 codes [14, 15].

As Table 6 illustrates, and for verification purposes, the numerical results were compared with those calculated from the ACI318-19 and AS 3600-2018 codes [14, 15].

5.1. Comparison with ACI318-19 code [14]

The stress and strain distributions for a RC beam cross section based on ACI 318-19 code [14] is shown in Fig. 9. Based on Fig. 9, Eq. (1) could be derived to calculate the nominal flexural strength M_n of PF lightweight concrete. From which P_u^{ACI} can be calculated, Table 6.

$$M_n = A_s f_y \left(d - 0.59 \frac{A_s f_y}{f_c^{'} b} \right) \quad (1)$$

$$M_n = 0.5 P_u . a \quad (2)$$

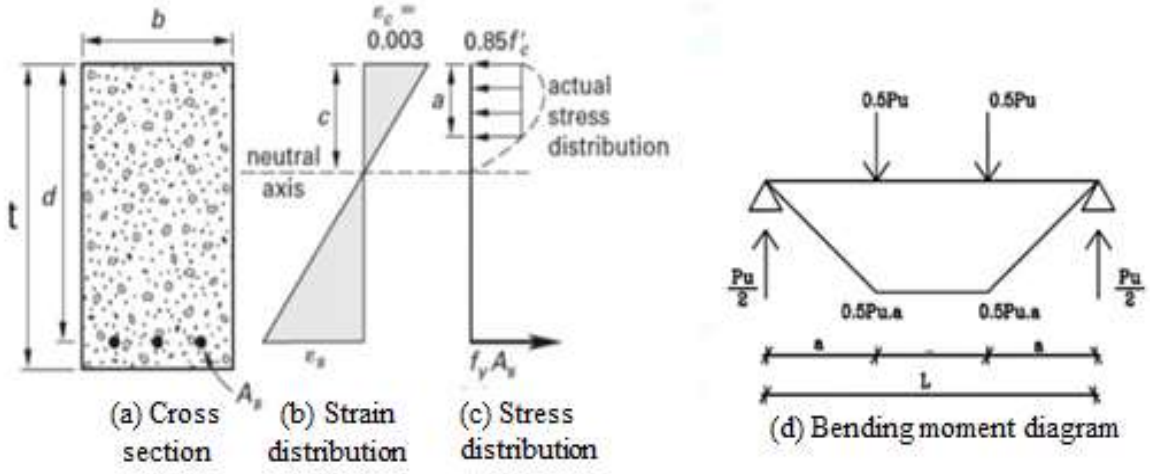

Fig. 9 Stress and strain distribution for RC beams based on ACI318-19 code [14].

Table 6 illustrates the comparison between the numerical ultimate load and the one calculated based on ACI318-19 code [14]. The mean of the ratio of the two ultimate loads is 105 %

and the standard deviation is 5.80 %. This comparison reveals good agreement between the numerical results and those calculated using the ACI318-19 code [14].

Table 6 P_u based on ACI 318-19 and AS 3600-2018 codes [14, 15] compared to numerical results.

Beam No.	Given data								Results					
	$f_c^{`}$ (MPa)	b (mm)	t (mm)	d (mm)	a (mm)	A_s actual (mm^2)	f_y (MPa)	A_{sc} (mm^2)	P_u^{ACI} (kN)	P_u^{AS} (kN)	$P_u^{\mathrm{NUM.}}$ (kN)	$\frac{P_U^{NUM.}}{P_u^{ACI}}$	$\frac{P_U^{NUM.}}{P_u^{AS}}$	$\frac{P_U^{ACI}}{P_u^{AS}}$
B1	26	100	300	260	600	149.2	400	56.00	49.02	51.72	54.6	1.11	1.06	0.95
B2	26	300	600	540	2000	1139.8	360	226.19	208.84	221.58	227.8	1.09	1.03	0.94
B3	26	300	600	540	2000	1519.8	360	226.19	272.79	295.44	276.1	1.01	0.93	0.92
B4	26	300	600	540	2000	1962.5	360	226.19	343.75	381.50	328.9	0.96	0.86	0.90
B5	26	300	600	540	2000	1139.8	400	226.19	230.47	246.20	242.5	1.05	0.98	0.94
B6	26	300	600	540	2000	1139.8	500	226.19	283.18	307.75	292.7	1.03	0.95	0.92
B7	26	300	600	540	2000	1139.8	600	226.19	333.92	369.30	332.5	1.00	0.90	0.90
B8	26	240	600	540	2000	1139.8	360	226.19	205.66	221.58	200.1	0.97	0.90	0.93
B9	26	360	600	540	2000	1139.8	360	226.19	210.96	221.58	242.5	1.15	1.09	0.95
B10	26	300	720	660	2000	1139.8	360	226.19	258.08	270.82	251.7	0.98	0.93	0.95
B11	26	300	840	780	2000	1139.8	360	226.19	307.32	320.06	335.0	1.09	1.05	0.96
B12	26	300	600	540	1500	1139.8	360	226.19	278.45	295.44	316.0	1.13	1.07	0.94
B13	26	300	600	540	2500	1139.8	360	226.19	167.07	177.26	170.0	1.02	0.96	0.94
Mean												1.05	0.98	0.93
Standard Deviation												0.06	0.07	0.02
Standard Deviation %												5.80	7.26	1.95

5.2. Comparison with AS 3600-2018 code [15]

Utilizing the stress block philosophy, the nominal flexural strength M_n of lightweight concrete based on AS 3600-2018 code [15] can be calculated from Eq. (3) as follows:

$$M_n = A_s f_y \left(d - \frac{\gamma k_u d}{2} \right) \tag{3}$$

in which k_u is a factor that can be calculated from Eq. (4) as follows:

$$k_u = \frac{A_s f_y}{\alpha_2 f_c^{'} \gamma b d + A_{sc} f_y} \tag{4}$$

where A_{sc} is the area of the compression steel and α_2 and γ can be calculated using Eqs. (5) and (6) as follows:

$$\alpha_2 = 0.85 - 0.0015 f_c^{'} \qquad \alpha_2 \geq 0.67 \tag{5}$$

$$\gamma = 0.97 - .0025 f_c^{'} \qquad \gamma \geq 0.67 \tag{6}$$

Table 6 illustrates the comparison between the numerical ultimate load and that calculated from AS 3600-2018 code [15]. The mean of the ratio of the two ultimate loads is 98 %

and the standard deviation is 7.26 %. Also, the comparison reveals good agreement between the numerical results and those calculated using the AS 3600-2018 code [15]. Clearly, the results of the ACI 318-19 code [14] are more closely related to the numerical results than those based on AS 3600-2018 code [15]. Also the results show that ACI 318-19 code [14] is more conservative than AS 3600-2018 code [15].

6. CONCLUSIONS

The nonlinear behavior of PF lightweight RC beams under flexure was numerically studied utilizing ANSYS program. For verification purposes, a nonlinear FE model was carried-out to simulate the behavior of beams previously tested by the author. The comparison between the numerical and the experimental results show that both are matched and good agreement was archived. After that, some variables which included the effect of main steel, steel yield strength, beam width, beam depth, and shear span were studied. Additionally, the numerical results were compared with those calculated based on ACI318-19 and AS 3600-2018 codes [14, 15]. The following are the main conclusions that can be drawn from the present study:

1. Nonlinear FE analysis simulates extently the experimental one.
2. For the considered beams, the higher the main steel, the higher the ultimate load, the higher secant stiffness and the lower the corresponding deflection.
3. Regarding the effect of steel yield strength, the initial part of the load deflection curves is approximately similar to that of the reference beam and varied nearest to the ultimate load according to the value of the steel yield strength.
4. The higher the yield strength, the higher the ultimate load, the higher secant stiffness and the lower the deflection at ultimate load.
5. The higher the beam depth and the beam width, the higher the ultimate load, the higher secant stiffness and the lower the deflection at ultimate load.
6. The higher the beam shear span, the less the ultimate load and deflection at ultimate load.
7. The mean and standard deviation demonstrate a good agreement between the numerical results and those based on ACI 318-19 and AS 3600-2018 codes [14, 15]. The results calculated based on ACI318-19 code [14] are more closely related to the numerical results than those of the AS 3600-2018 code [15].
8. The results show that ACI 318-19 code [14] is more conservative than AS 3600-2018 code [15].

7. REFERENCES

1-ACI-213, Guide for structural lightweight-aggregate concrete, ACI Committee ,213 American Concrete Institute, Farmington Hills, Michigan, USA: ISBN: 978-0-87031-897-9; 2014.

2-Mukhopadhyay, S., and Khatan, A. S., "A Review on the Use of Fibers in Reinforced Cementitious Concrete," Journal of Industrial Textiles, 2015, 45.2: 239-264.

3-Aziz, M. A., Paramasivam, P., and Lee, S. L., "Prospects for Natural Fiber Reinforced Concretes in Construction, "International Journal of Cement Composites and Lightweight Concrete, 3.2 (1981): 123-132.

4-Badogiannis, E. G., Christidis, K. I., and Tzanetatos, G. E., “Evaluation of the Mechanical Behavior of Pumice Lightweight Concrete Reinforced with Steel and Polypropylene Fibers,” Construction and Building Materials, 2019,196, 443-456.

5-Srinivasu, V., and Padmavathi, N. V., "An Experimental Investigation on Strength Properties of Polypropylene Fibers," IJESRT Journal of Engineering Sciences ,2018, Vol.7, no.12, 419-436.

6- Gencel, O., Ozel, C., Brostow, W., and Martinez, B., G., "Mechanical properties of self-compacting concrete reinforced with polypropylene fibers," Journal of Materials Research Innovations, 2011, 15(3), 216-225.

7- Mazaheripour, H., Ghanbarpour, S., Mirmoradi, S. H., and Hosseinpour, I., "The effect of polypropylene fibers on the properties of fresh and hardened lightweight self-compacting concrete," Journal of Construction and Building Materials, 2011, 25(1), 351-358.

8- Altalabani, D., Bzeni, D. K., & Linsel, S., "Mechanical properties and load deflection relationship of polypropylene fiber reinforced self-compacting lightweight concrete," Construction and Building Materials, 2020, 252, 119084.

9-Bangash, M. Y. H.,” Concrete and Concrete Structures: Numerical Modeling and Applications,” 1989.

10-Hemmaty, Y., “Modeling of the Shear Force Transferred Between Cracks in Reinforced and Fiber Reinforced Concrete Structures,” International Proceedings of the ANSYS Conference, Pittsburgh, Pennsylvania, August, 1998, p. 201-209.

11-Musmar, M., “Nonlinear Finite Element Flexural Analysis of RC Beams,” International Journal of Applied Engineering Research, 2018, 13.4: 2014-2020.

12-Tjitradi, D., Eliatun, E., and Taufik, S., “3-D ANSYS Numerical Modeling of Reinforced Concrete Beam Behavior under Different Collapsed Mechanisms,” International Journal of Mechanics and Applications, 2017, 7.1: 14-23.

13-Amna, H. A., Amr, H. Z., and Wael, M. M., "Shear Behavior of Reinforced Lightweight Concrete T-Beams," Life Science Journal, 2019, 16.8: 11-31.

14-ACI Committee 318-19, Building Code Required for Reinforced Concrete, (ACI 318-19) and Commentary (ACI 318R-19), American Concrete Institute, Farmington Hills, Mich,2019.

15-AS 3600-2018, Concrete Structures, Standards Australia Limited, Sydney, Google Scholar.

16-ANSYS Inc., Release 15.0, Documentation, Theory References, 2013.

17- Shimaa, M. M., "Flexural Behavior of Hybrid Polypropylene Fiber Reinforced Structural Lightweight Concrete Beams," M.Sc. (under Discussion), Structural Engineering Department, Faculty of Engineering, Mansoura University, Egypt, 2021.